Design of H_∞ loop-shaping controllers for fluid power systems

I A Njabeleke, R F Pannett, P K Chawdhry and **C R Burrows***
Centre for Power Transmission and Motion Control, Faculty of Engineering and Design, University of Bath, UK

Abstract: Fluid power systems are highly non-linear, making the application of traditional linear feedback control techniques challenging. In this paper, a dual-mode H_∞ control scheme has been proposed and demonstrated to be both feasible and practical for controlling such systems. The plant used is a speed control hydrostatic transmission and the particular H_∞ approach used is loop shaping as suggested by McFarlane and Glover; this, in addition to simplicity, admits a wider class of uncertainties than comparable schemes. The dual-mode controller is surprisingly effective, delivering robust stability over the entire speed range and offering bumpless transfer, wind-up protection and multi-rate sampling at little extra cost, a factor which is crucial in digital implementation. It is shown that, despite some challenges, a successful H_∞ controller need not be of high order.

Keywords: H_∞, loop shaping, fluid power, hydrostatic transmission

NOTATION

A	steady state offset
A, **B**, **C**, **D**	state space representation of **G**
$\boldsymbol{d}$	disturbance signal (vector)
e	error
f, f_i	anti-wind-up and bumpless transfer scheme gains
$G(s)$	transfer function
G	transfer function matrix
G_d	disturbance dynamics (scalar)
$\mathbf{G}_\mathrm{d}$	disturbance dynamics (matrix)
$\mathbf{G}_\mathrm{p}$	perturbed model of plant
I	identity matrix
k_i	alternative controllers, bumpless transfer scheme
K	controller (scalar)
K	controller (matrix)
M	peak value of S
M, **N**	left coprime factors of **G**
P	plant
$\boldsymbol{r}$	reference signal
s	complex variable, Laplace
S	sensitivity function (scalar)
S	sensitivity function (matrix)
t_s	sampling interval
T	complementary sensitivity function (scalar)
T	complementary sensitivity function (matrix)
u	control signal
u_c	controller output
$u_\mathrm{max}, u_\mathrm{min}$	saturation limits on plant input
w_p	performance weight
W_del	uncertainty weight
W_p	performance weight
W_1	pre-compensator weight
W_2	post-compensator weight
y	output
$\boldsymbol{y}_\mathrm{d}$	output due to disturbance
$\boldsymbol{y}_\mathrm{r}$	output due to reference
z	zero in the s plane
z	complex variable, discrete time
Δ	uncertainty
ϵ	stability margin
ρ	spectral radius
$\overline{\sigma}(\ )$	maximum singular value
ϕ	coprime factor model equation error
ω	angular frequency
ω_B	closed-loop bandwidth
$\|.\|_\mathrm{H}$	Hankel norm
$\|.\|_\infty$	infinity norm

The MS was received on 2 April 1998 and was accepted after revision for publication on 8 March 1999.
* *Corresponding author: Centre for Power Transmission and Motion Control, Faculty of Engineering and Design, University of Bath, Claverton Down, Bath BA2 7AY, UK*

1 INTRODUCTION

The attractive properties of fluid power systems are well known [**1**], and this form of energy transmission is frequently used in applications where high power density is

important. Unfortunately, it is not always possible to satisfy all system requirements such as a high speed of response, variable-speed operation and disturbance rejection in the face of model uncertainty and supply pressure variations, in open loop. This is particularly the case if a wide range of operating speeds (flexibility) is required. Therefore increasing use has been made of feedback control. Feedback control theory is only fully developed for linear systems whereas fluid power systems are characterized by severe non-linearities and model uncertainty. The primary aim of this work is to develop a controller that is capable of robustly satisfying disturbance rejection and set point tracking requirements in the face of the aforementioned problems over a range of operating speeds. In the process, the aim is to minimize the complexity of the controller.

The plant under study is a servo-valve-controlled axial piston motor driving a loaded hydraulic pump. The pump is used to simulate load disturbance duty cycles which the motor will normally be used to support in a typical manufacturing process. The objectives are to achieve rapidly a desired motor speed and to maintain accurately the desired speed while driving loads which perform various duty cycles.

In addition to load uncertainties and general non-linearities, there is also an unpredictable variation in supply pressure. In practice this tends to be caused by other loads feeding off the pressure supply mains or simply the inability of the supply system to maintain a constant pressure in the presence of a time-varying load.

Section 2 examines the modelling problems involved in the speed control process and presents an introduction to a software environment for detailed modelling of fluid power systems. It also examines the special problems that arise, by investigating the process characteristics. Section 3 presents the motivation for robust control and shows the advantages of loop shaping. Section 4 deals with the design process using loop shaping. As well as considering the digital implementation aspects, using μ analyses a comparison of the robust performance of the loop-shaping controller is made with a proportional–integral–derivative (PID) controller. Section 5 contains experimental results from the test rig. Finally, the conclusions of this research are presented in Section 6.

2 PROCESS MODELLING AND PROCESS CHARACTERISTICS

2.1 Process modelling

Modelling a complete fluid power system from first principles is not straightforward. It is made even more difficult if the model is to be used for system design, for it must then facilitate the changing of components and parameters. Even if it were possible to obtain the full non-linear models, the utility of this in control design would be limited as the only analytical techniques which make full use of the non-linear models, namely differential geometric techniques [**2**, **3**], are vulnerable to uncertainty, both structured and parametric. In these circumstances, recourse is made to linear control based on approximate numerical models. In this respect, the software package, BATH*fp*, developed at the University of Bath, has been found to be extremely useful. This is a simulation package for the analysis and design of fluid power systems [**4**]. The user defines the circuit to be analysed on a computer screen in much the same way as a draughtsman produces a schematic drawing (Fig. 1). After relevant parameters have been entered, the circuit can be simulated directly and the results obtained. Most importantly, it is possible to obtain an approximate linear model of the system at any specified point in state space. This facility makes the package an ideal tool for designing and assessing linear controllers as the controller can be included in the simulation in the same way as other model components.

There are two levels of uncertainty in the approximate linear models. Firstly, there is a degree of uncertainty in modelling the physical plant, e.g. because valve and motor characteristics (data) are only given by

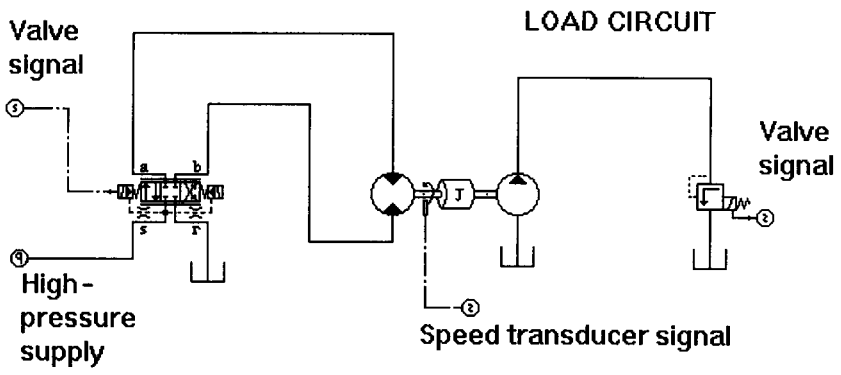

Fig. 1 Speed control of a hydraulic motor: BATH*fp* schematic diagram

manufacturers at fixed operating points and, even then, only approximately. This type of uncertainty is difficult to quantify. Secondly, even if full knowledge of the plant were available, the plant non-linearities represent uncertainty when seen from the viewpoint of a linear model. This type of uncertainty is easier to deal with because at least a quantitative idea of its value can be obtained numerically by studying the linear approximations produced by a simulation. In this application, other factors such as frictional effects were ignored as it was difficult to estimate them in a reliable way. In some applications, this simplification may not be justified, and it is well known that the estimation of frictional effects poses challenging problems.

In control terms, the example is represented as a speed control problem. The load torque can only be delivered if the speed of the pump is maintained. The load duty cycle is treated as a disturbance in the output. Thus fast tracking of reference inputs is required but also adequate disturbance rejection is essential.

Using BATH*fp*, a series of linear models spanning the operating envelope, and in particular, covering different levels of speed and supply pressure is obtained for the plant in Fig. 1. The supply pressure ranges from 30 to 100 bar and the speed ranges from that corresponding to 5 per cent of valve opening to 80 per cent of valve opening. These conditions represent a very wide range of operation.

Figure 2 shows the singular value plots (effectively magnitude plots, as this is a single-input single-output system) for the open-loop system. In general, the higher the supply pressure, the higher is the system gain.

2.2 Process characteristics

A study of the linear approximations in Fig. 2 exposes certain characteristics which are typical in fluid power:

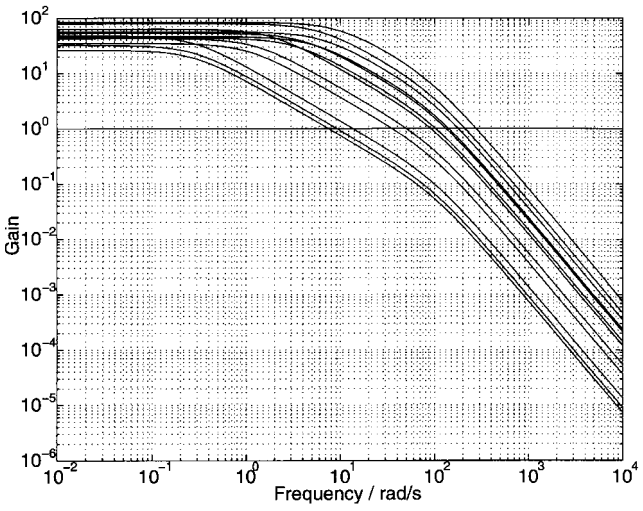

Fig. 2 Singular value plots for a family of linear approximations

1. *Large model variations at the different operating points*. Distance measures using the gap and η-gap metrics [**5**] returned high values (greater than 0.9) for the unweighted plant, suggesting large model variation and indicating that a controller designed for one set of operating conditions will have to be extremely robust to stabilize the plant at different operating points. This can be attributed to the highly non-linear nature of the system. In addition to the non-linear characteristics of the fluid power components, variations in the fluid properties such as compressibility and viscosity introduce further complexity.
2. *Large bandwidth variations*. The bandwidth varies by an order of magnitude over the complete speed range. This can be critical in a digital implementation. A sampling rate appropriate for the high-speed action may be too high for low-speed action, leading to numerical problems (considered further in Section 5.1). This calls for careful thought in the final digital implementation.
3. *Right half-plane (RHP) zeros*. RHP zeros are a major concern in any system which is to have a large bandwidth. This is because they present hard upper and lower limits to the achievable bandwidth.

To characterize these limitations, Zames' [**6**] sensitivity peak will be used as follows. Suppose that the transfer function $G(s)$ has an RHP zero z and let w_p be any stable minimum-phase weight. Then, for closed-loop stability, the weighted sensitivity function must satisfy

$$\left\|w_\mathrm{p}S\right\|_\infty \geqslant \left|w_\mathrm{p}(z)\right|$$

The proof can be found in reference [**6**].

For the trivial weight $w_\mathrm{p}(s) = 1$, it is required that $\|S\|_\infty \geqslant 1$, which must hold for any real system as $|S|$ must approach unity at high frequencies. However, a much deeper insight could be gained by adopting choices of weight other than unity.

For performance, it is necessary that

$$\left\|w_\mathrm{p}S\right\|_\infty < 1 \Leftrightarrow |S(\mathrm{j}\omega)| < \frac{1}{\left|w_\mathrm{p}(\omega)\right|}, \qquad \forall\omega$$

If an attempt is made to select good weights for low- and high-frequency performance (following the guidelines presented in Section 3), it is immediately discovered that there is a limitation on both high- and low-frequency performance. Consider, for example, the weight

$$w_\mathrm{p}(s) = \frac{s/M + \omega_\mathrm{B}}{s + \omega_\mathrm{B}A}$$

which specifies a minimum bandwidth ω_B, a maximum peak of $|S|$ of M, a steady state offset less than $A < 1$ and, at frequencies lower than the bandwidth, the sensitivity is required to improve by at least 20 dB/decade.

If there is a real RHP zero at $s = z$, then, to satisfy $\|w_p S\|_\infty < 1$, an easy calculation shows that it is necessary at least that $\omega_B(1 - A) < z(1 - 1/M)$. Specifically, for $A = 0$ (no offset) and $M = 2$, $\omega_B < 0.5z$.

For a zero on the imaginary axis, $s = j|z|$, it is necessary at least that $\omega_B < |z|\sqrt{1 - 1/M^2}$, or, for $M = 2$, $\omega_B < 0.86|z|$. Thus the low-frequency operation is limited to below the frequency of the RHP zero.

Suppose now that there must be tight control at high frequencies. Then the following type of weight is considered:

$$w_p(s) = \frac{1}{M} + \frac{s}{\omega_B}$$

This requires tight control ($|S(j\omega)| < 1$) at frequencies higher than ω_B whereas the only requirement at low frequencies is that the peak of $|S|$ be less than M. Then, to satisfy $\|w_p S\|_\infty < 1$ with a real RHP zero,

$$\omega_B > z\frac{1}{1 - 1/M}$$

With $M = 2$, for example, the requirement is $\omega_B > 2z$. Thus tight control can only be achieved at high frequencies beyond the frequency of the RHP zero.

In addition to these bandwidth limitations, extra problems arise. RHP zeros make the systems of a non-minimum phase nature and thus call for caution when considering cancellation-based control schemes such as linear quadratic Gaussian with loop transfer recovery. Additional problems include internal stability; the controller cannot remove the effect of the RHP zero by placing an unstable pole at the corresponding location. Thus, if G has an RHP zero at z (real or complex), then the complementary sensitivity function T also has an RHP zero at z. Another type of behaviour which can be significant is inverse response, namely that the response initially goes the 'wrong way' before eventually going the 'right way'.

3 H_∞ ROBUST CONTROL FOR FLUID POWER SYSTEMS

3.1 Motivation for H_∞

As has been seen, component characteristics are non-linear and a high level of model uncertainty comes from the modelling process. This means that, even if the non-linear models were available, techniques such as differential geometry which make full use of the non-linear models and are based on non-linear transformations could not be used, as they are highly sensitive to uncertainties. Other possible non-linear techniques such as variable structure control [7] call for extremely high switching frequencies as well as utilizing full state measurements, which are not always available. Techniques such as artificial neural networks are mainly statistical and impossible to analyse or assess, save by repeated simulation (as with other non-linear techniques). Other linear techniques likewise, while they may be reasonably robust, do not have the assurance of a guaranteed robustness margin in the face of non-linearities and are not easily extendable to multiple-input multiple-output systems. This leaves robust H_∞ control as the prime candidate for this type of system, particularly since acceptable performance is required over various loads, speeds, supply pressure and other operating parameters. In addition to allowing the possibility of actually providing a guaranteed level of performance for a given set of conditions and perturbations, H_∞ is naturally applicable to multiple-input multiple-output systems.

H_∞ control has been considered for fluid power systems in the past [8, 9]. However, despite interesting simulation results [10], there have been few reported practical applications [11]. The reasons cited for this have been mainly the difficulty in weight selection and the perceived necessity for high-order controllers. The paucity of applications also means that specific problems that may arise during a practical application have not been addressed. In this paper, it is shown that the concerns generally cited about the implementation of H_∞ control are not necessarily valid.

3.2 Linear system design considerations

Stating the appropriate controller characteristics to satisfy different requirements for linear systems is straightforward. Consider the feedback system in Fig. 3.

The following general characteristics can be stated [12, 13]. A good performance requires that the collection

$$\overline{\sigma}(\mathbf{I} + \mathbf{PK})^{-1} = \overline{\sigma}(\mathbf{S})$$

$$\overline{\sigma}[(\mathbf{I} + \mathbf{PK})^{-1}\mathbf{P}]$$

$$\overline{\sigma}(\mathbf{I} + \mathbf{KP})^{-1}$$

$$\overline{\sigma}[\mathbf{K}(\mathbf{I} + \mathbf{PK})^{-1}]$$

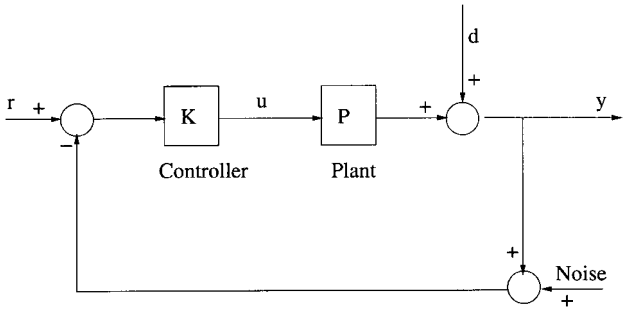

Fig. 3 One-degree-of-freedom feedback configuration

be made small, particularly in some low-frequency range where $\boldsymbol{d}$ is likely to be significant. On the other hand, good robustness requires that the collection

$$\overline{\sigma}[\mathbf{PK}(\mathbf{I}+\mathbf{PK})^{-1}] = \overline{\sigma}(\mathbf{T})$$

$$\overline{\sigma}[\mathbf{KP}(\mathbf{I}+\mathbf{KP})^{-1}]$$

be made small, particularly in some high-frequency range. H_∞ works by looking for a controller that modifies these functions to achieve the relevant objectives.

The sensitivity function $\mathbf{S}$ and the complementary sensitivity function $\mathbf{T}$ predict the performance, with respect to disturbance rejection and tracking respectively, of the closed-loop system. Indeed, the effect of the disturbance $\boldsymbol{d}$ on the output is simply $\|\boldsymbol{y}_\mathrm{d}(\mathrm{j}\omega)\| = \|\mathbf{S}(\mathrm{j}\omega)\|\|\boldsymbol{d}(\mathrm{j}\omega)\|$ (i.e. to reduce the effect of disturbance, make $\mathbf{S}$ as small as possible, ideally zero) and the effect of the reference signal $\boldsymbol{r}$ on the output is simply $\|\boldsymbol{y}_\mathrm{r}(\mathrm{j}\omega)\| = \|\mathbf{T}(\mathrm{j}\omega)\|\|\boldsymbol{r}(\mathrm{j}\omega)\|$ (i.e. for good tracking, make $\mathbf{T}$ as close to unity as possible). Note, however, that in general the disturbance will be associated with some disturbance dynamics $\mathbf{G}_\mathrm{d}$; thus the actual contribution of the disturbance to the output is $\|\boldsymbol{y}_\mathrm{d}(\mathrm{j}\omega)\| = \|\mathbf{G}_\mathrm{d}(\mathrm{j}\omega)\mathbf{S}(\mathrm{j}\omega)\|\|\boldsymbol{d}(\mathrm{j}\omega)\|$.

3.3 H_∞ loop shaping

Several approaches are available for H_∞ control design. However, over recent years, the H_∞ loop-shaping approach of McFarlane and Glover [**14**] has emerged as the preferred practical approach to robust control design. It overcomes the 'complicated' weight selection process in the time domain design, the restrictions and inconvenience of mixed sensitivity and also avoids the iteration schemes associated with μ synthesis [**12**]. The idea is simple; the open-loop response is shaped to satisfy the performance requirements such as tracking and disturbance rejection, and then an H_∞ controller is designed to stabilize the shaped plant. The H_∞ controller is purely for robustness and is designed to give the maximum stability margins possible for the selected weights. What is more, for a good design, it hardly changes the closed-loop singular values. The perturbation structure is based on normalized coprime factors and is very suitable for parametric uncertainty (Fig. 4). In loop shaping, the stabilization of the plant $\mathbf{G}$, which has a normalized left coprime factorization $\mathbf{G} = \mathbf{M}^{-1}\mathbf{N}$, is considered. A perturbed model of the plant $\mathbf{G}_\mathrm{p}$ can then be written as $\mathbf{G}_\mathrm{p} = (\mathbf{M}+\Delta_\mathbf{M})^{-1}(\mathbf{N}+\Delta_\mathbf{N})$, where $\Delta_\mathbf{M}$ and $\Delta_\mathbf{N}$ are stable unknown transfer functions which represent the uncertainty in the nominal plant model $\mathbf{G}$. The objective of robust stabilization is to stabilize not

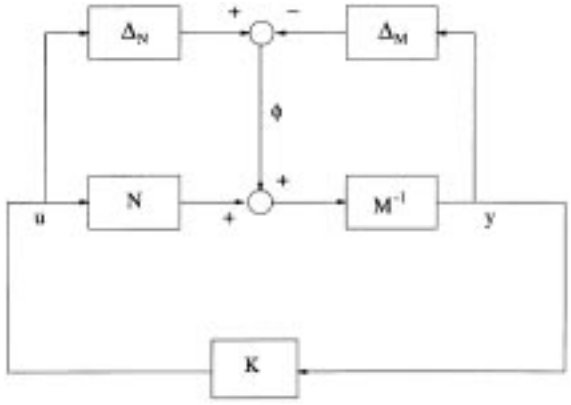

Fig. 4 H_∞ robust stabilization problem

only the nominal model $\mathbf{G}$ but also a family of perturbed plants defined by

$$\mathbf{G}_\mathrm{p} = \left\{(\mathbf{M}+\Delta_\mathbf{M})^{-1}(\mathbf{N}+\Delta_\mathbf{N}) : \|[\Delta_\mathbf{N}\Delta_\mathbf{M}]\|_\infty < \epsilon\right\}$$

where $\epsilon > 0$ represents the stability margin. The job of the loop shaping algorithm is to maximize this stability margin, thus maximizing the amount of admissible perturbation.

For the perturbed feedback system shown in Fig. 4, the stability property is robust if and only if the nominal feedback system is stable and

$$\gamma \triangleq \left\| \begin{bmatrix} \mathbf{K} \\ \mathbf{I} \end{bmatrix} (\mathbf{I}-\mathbf{GK})^{-1}\mathbf{M}^{-1} \right\|_\infty \leqslant \frac{1}{\epsilon}$$

where γ is the H_∞ norm from ϕ to $\binom{\boldsymbol{u}}{\boldsymbol{y}}$ and $(\mathbf{I}-\mathbf{GK})^{-1}$ is the sensitivity function for this positive feedback arrangement. The lowest achievable γ and the corresponding maximum stability margin ϵ are given by

$$\gamma_{\min} = \epsilon_{\max}^{-1} = \left(1 - \|[\mathbf{N} \quad \mathbf{M}]\|_\mathrm{H}^2\right)^{-1/2} = [1+\rho(\mathbf{XZ})]^{1/2}$$

In fact a controller which satisfies

$$\left\| \begin{bmatrix} \mathbf{K} \\ \mathbf{I} \end{bmatrix} (\mathbf{I}-\mathbf{GK})^{-1}\mathbf{M}^{-1} \right\|_\infty \leqslant \gamma$$

for a specified $\gamma \geqslant \gamma_{\min}$ is given by

$$\mathbf{K} = \begin{bmatrix} \mathbf{A} + \mathbf{BF} + \gamma^2 (\mathbf{L}^{\mathrm{T}})^{-1} \mathbf{Z}\mathbf{C}^{\mathrm{T}}(\mathbf{C} + \mathbf{DF}) & \gamma^2 (\mathbf{L}^{\mathrm{T}})^{-1} \mathbf{Z}\mathbf{C}^{\mathrm{T}} \\ \mathbf{B}^{\mathrm{T}}\mathbf{X} & -\mathbf{D}^{\mathrm{T}} \end{bmatrix}$$

$$\mathbf{F} = -\mathbf{S}^{-1}(\mathbf{D}^{\mathrm{T}}\mathbf{C} + \mathbf{B}^{\mathrm{T}}\mathbf{X})$$

$$\mathbf{L} = (\mathbf{1} - \gamma^2)\mathbf{I} + \mathbf{XZ}$$

where $\mathbf{Z}$ is the unique positive definite solution to the algebraic Riccati equation

$$(\mathbf{A} - \mathbf{BS}^{-1}\mathbf{D}^{\mathrm{T}}\mathbf{C})\mathbf{Z} + \mathbf{Z}(\mathbf{A} - \mathbf{BS}^{-1}\mathbf{D}^{\mathrm{T}}\mathbf{C})^{\mathrm{T}} - \mathbf{ZC}^{\mathrm{T}}\mathbf{R}^{-1}\mathbf{CZ} + \mathbf{BS}^{-1}\mathbf{B}^{\mathrm{T}} = \mathbf{0}$$

where $\mathbf{S} = \mathbf{I} + \mathbf{D}^{\mathrm{T}}\mathbf{D}$ and $\mathbf{X}$ is the unique positive definite solution to the algebraic Riccati equation

$$(\mathbf{A} - \mathbf{BS}^{-1}\mathbf{D}^{\mathrm{T}}\mathbf{C})\mathbf{X} + \mathbf{X}(\mathbf{A} - \mathbf{BS}^{-1}\mathbf{D}^{\mathrm{T}}\mathbf{C}) - \mathbf{XBS}^{-1}\mathbf{B}^{\mathrm{T}}\mathbf{X} + \mathbf{C}^{\mathrm{T}}\mathbf{R}^{-1}\mathbf{C} = \mathbf{0}$$

and $\{\mathbf{A}, \mathbf{B}, \mathbf{C}, \mathbf{D}\}$ is the minimal state space realization of $\mathbf{G}$. Note that, for a strictly proper plant, $\mathbf{D} = \mathbf{0}$ and the formulae simplify considerably. The closed-loop system will be stable provided that $[\triangle_{\mathbf{M}} \quad \triangle_{\mathbf{N}}]$ is stable and has incremental gain less than γ^{-1}, a generalization which admits non-linear and time-varying perturbations.

The cost function in this controller, as well as robust stability, also has robust performance interpretations and it is not atypical for loop shape designs to yield robust performance the first time! Note that the normalized coprime factor uncertainty representation has no restriction on the number of RHP poles and is thus capable of representing a wider class of systems than the multiplicative or additive model structures [which for example cannot represent uncertain resonances (poles on the imaginary axis)] normally used to represent model uncertainty. Due to the close similarity to classical loop shaping, the weight selection process is particularly simple and intuitive as it is hardly different from (since only gain compensation is considered, it is indeed easier than) the standard cascade compensation in linear system design.

4 CONTROL SYSTEM DESIGN

4.1 Uncertainty description

From the profiles of frequency responses (Fig. 2), it is possible to form an idea of the plant uncertainty. One way of approaching the uncertainty is to measure the η gap between all the models. The η gap measure between the most widely separated plants is close to unity. A possible way to deal with the uncertainty is to select some mid-point transfer function and to try to maximize the robustness in the hope that it will stabilize all the plants. While this method may achieve robust stability (by settling for a sufficiently small loop gain), it may not achieve adequate performance at all the operating points of interest. What is more, the set of characteristics can be usefully divided into two: one set corresponding to low speeds and one set corresponding to medium to high speeds. Then the η gap between systems in the same set is considerably reduced (of the order of 0.5). This motivates a multi-mode controller for this problem, made up of two controllers: one for high speeds and one for low speeds. Interestingly, a multi-mode scheme confers numerous other advantages on the design:

1. Performance can be optimized at different speeds as different limitations apply.
2. The overall stability margin is higher since more than one robust controller is used.
3. The different controllers could be sampled at different rates at little additional cost. This is important since the bandwidths are very different and a uniform sampling rate over all speeds could lead to numerical problems.
4. The bumpless transfer scheme used achieves integral wind-up protection at no extra cost.

Obviously, the smaller the number of controllers in a multi-mode controller, the cheaper and simpler is the design. Two controllers (one for high speed and one for low speed) were found to be quite adequate for this particular problem. Note that, for a given valve opening, the motor speed will depend on the supply pressure. Thus, in the following analyses, low speed is used to describe valve openings of under 20 per cent while high speed is used for valve openings over 20 per cent.

4.2 Design

4.2.1 Disturbance dynamics

The primary aim is to maximize disturbance rejection across the speed range so that the motor can drive various loads in the duty cycle at any speed. The disturbance behaviour is difficult to measure because it depends on the speed, supply pressure and magnitude of the disturbance. However a rough idea of the behaviour can be obtained by using the same procedure that was used for modelling in Section 2.1, to calculate a family of disturbance dynamics. The disturbance transfer function G_{d} from disturbance input to plant output is examined.

Figure 5 shows gain plots for the family of disturbance transfer functions at various speeds (or rather

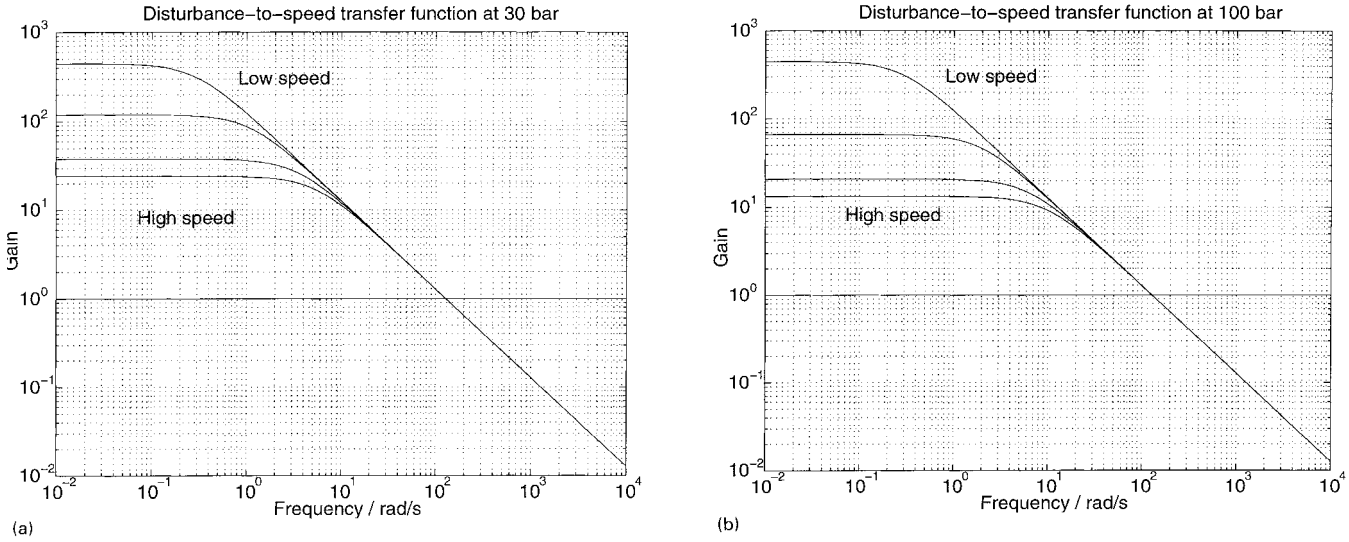

Fig. 5 Singular value plots for families of disturbance transfer functions: (a) 30 bar; (b) 100 bar

valve openings). The disturbance-to-speed transfer functions are lower at higher supply pressures than at lower pressures. Also, they are lower for higher speeds than for lower speeds. As a result, the disturbance rejection should improve both with an increase in supply pressure and with an increase in speed. However, what is really important in these plots is the fact that the disturbance transfer functions begin to fall rapidly from around 0.2 rad/s. Thus an increase in sensitivity from around this frequency could be tolerated.

As stated, loop shaping simply consists of shaping the open loop in the classical sense and then designing a robustly stabilizing feedback controller. Another examination of the plots in Fig. 2 shows that all the plots have the rather favourable roll-off (from -15 to about -30 dB/decade) around crossover. Thus a simple proportional–integral (PI) pre-compensator should be adequate to achieve the required closed-loop behaviour. Integral action is particularly important as it boosts the low-frequency gain, leading to a reduction in the steady state error. In selecting the loop gain, the extra uncertainty that represents the difference between the nonlinear model in BATH*fp* and the actual plant needs to be considered. In addition, the loop gain should not be so high as to enable the RHP zeros to have a significant effect on performance.

The zeros of the high-speed plant are

$$10^9 \times \begin{bmatrix} 0.000\,006\,3 + 3.3175\mathrm{j} \\ 0.000\,006\,3 - 3.3175\mathrm{j} \\ -7.66 \times 10^{-5} \\ -1.035 \times 10^{-6} \\ -7.505 \times 10^{-6} \end{bmatrix}$$

and those of the low-speed plant are

$$10^8 \times \begin{bmatrix} -6.425\,6 \\ 6.428\,85 \\ -0.0135 \\ -1.035 \times 10^{-4} \\ -7.489 \times 10^{-5} \end{bmatrix}$$

To be able to attenuate all disturbances, the loop gain must be selected such that $|S| < 1$ over the relevant frequency range (in this case between 0 and 0.2 rad/s at least). For the high-speed controller, a PI pre-compensator $W_1 = 0.5(s+1)/s$ was used to boost the low-frequency gain, thereby removing offset. Let the post-compensator $W_2 = 1$. This combination gave an acceptable sensitivity peak and returned a γ of 1.81. For the low-speed controller, we used the pre-compensator $W_1 = 0.08(s+1)/s$ due to the much lower roll-off rate of the system around crossover. The post-compensator is still set at $W_2 = 1$ and the obtained γ was 1.67. Figure 6 shows the singular value plots with compensations for both controllers.

A robust stabilizing one degree-of-freedom controller was designed for both systems. The implementation used was that of a forward path compensator as shown in Fig. 7.

4.2.2 *Model reduction*

Both the high- and the low-speed controllers were found to have nine states (including the PI weight). However, many of these states were nearly unobservable and so had little effect on the input–output behaviour. It was thus possible to obtain reduced-order controllers. Model

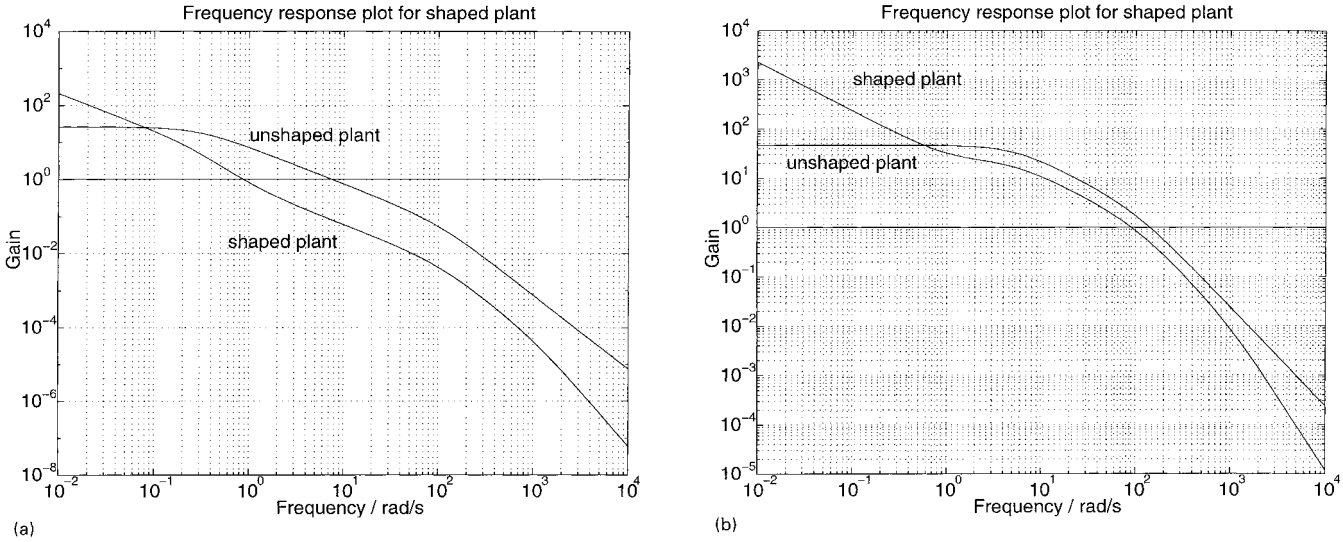

Fig. 6 Singular value plots for shaped plants: (a) low speeds; (b) high speeds

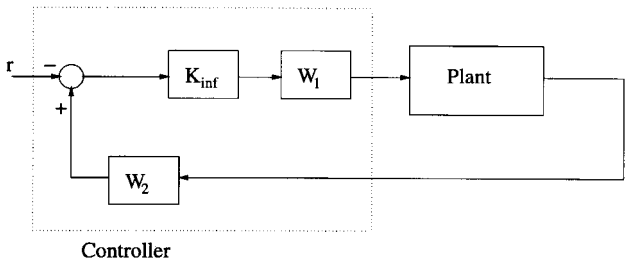

Fig. 7 Implementation of stabilizing loop-sharing controller

reduction was performed on the controller using the technique of *balanced residualization* (see, for example, reference [**12**]). The *balancing* removes the uncontrollable and unobservable states while the *residualization* discards the dynamics of very fast states via singular perturbation approximation. This approach offers good low-frequency performance (in fact the d.c. gain is maintained) as well as a reasonable medium-frequency approximation. Very-high-frequency performance is not crucial since the design bandwidth is limited. The Hankel singular values provide a guide to the number of states which may be removed. For the high-speed controller (after balancing) they were $\{0.606, 0.244, 0.113, 3.915 \times 10^{-4}, 1.837 \times 10^{-6}, 4.44 \times 10^{-12}, 2.09 \times 10^{-12}\}$. For the low-speed controller, they were $\{0.674, 0.044, 1.733 \times 10^{-3}, 1.905 \times 10^{-6}, 1.39 \times 10^{-10}\}$. The high- and low-speed controllers were reduced to three and four states respectively with no significant deterioration in performance. Figure 8 shows singular value plots for both reduced- and full-order controllers for high and

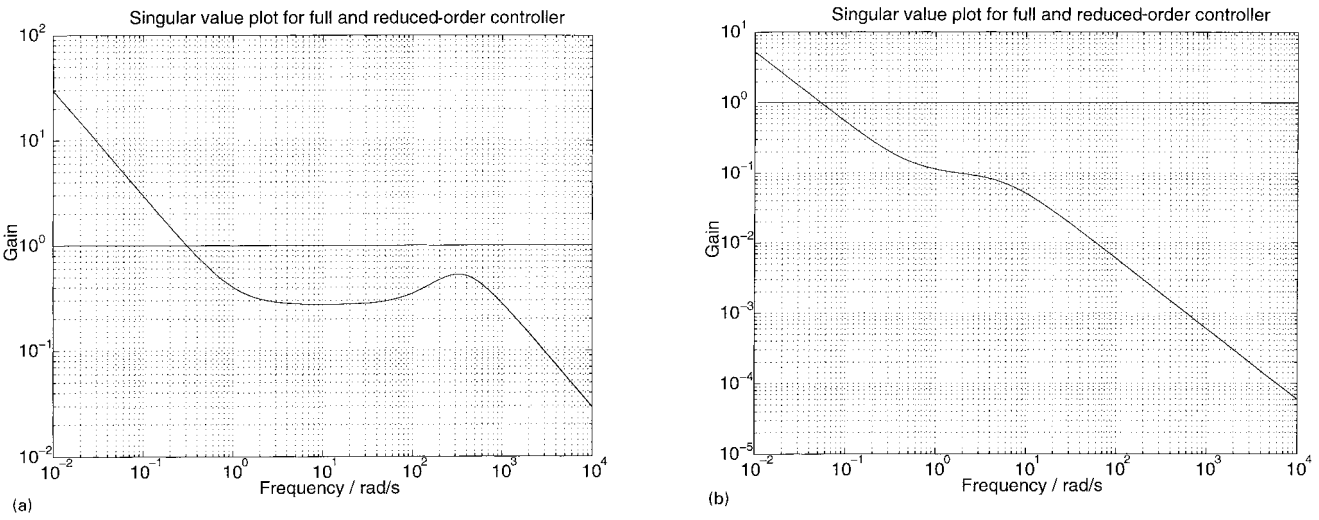

Fig. 8 Model reduction of controller: (a) high speeds; (b) low speeds

low speeds. The plots of the reduced- and full-order controllers are virtually indistinguishable.

4.3 Controller characteristics

Figure 9 shows a plot of the sensitivity function as well as some tracking and disturbance rejection action of the low- and high-speed controllers. Note the reduced bandwidth of the low-speed controller. Thus, while this controller will stabilize the plant at high speeds (due to its low gain), the performance will be rather poor due to the corresponding reduction in bandwidth. Figure 9c shows the actual effect on output disturbances as it takes account of the disturbance dynamics. Note the decrease in the disturbance-to-speed transfer function (compared with the open-loop values in Fig. 5) as a result of closing the loop. For the low-speed controller, the worst disturbance rejection performance (occurring at about 1 rad/s) is a reduction of 11.5 dB on the d.c. value (in fact, this particular reduction is due to the natural roll-off of the disturbance dynamics). For the high-speed controller, the worst-case performance is an impressive 47 dB on the d.c. value.

4.3.1 *Bumpless transfer and integrator wind-up protection*

Whenever a multi-mode controller is used to control a process, care must be taken to ensure that no adverse transient effects occur when a controller switch occurs (i.e. a bumpless transfer is desired). This is done by conditioning all off-line controllers so that their outputs and states are compatible with the process at the instant of engagement. Several designs of bumpless transfer schemes are possible and, before considering one such design, first an anti-wind-up scheme is introduced. Even though the focus is on the bumpless transfer scheme, an anti-wind-up scheme is invariably a practical necessity in the presence of integral action.

Whenever there is a large error due to a large set point change, the demand signal into the servo-valve will be large (due to the large controller gain), typically greater than the maximum specified input current of the servo-valve. This will cause the controller to saturate and, if there were then a decrease or reversal of error due to an opposed demand, the input would stay in saturation for a considerable amount of time, leading to an unacceptable transient. To solve this problem, the following anti-wind-up scheme is used [**15**].

The scheme consists of a feedback loop around the controller (Fig. 10a) that is activated as soon as $u > u_{\max}$ (or less than $u_{\min}$). If $u = u_c$, then everything proceeds in a normal linear manner. If, however, u saturates at $u_{\max}$, (or alternatively $u_{\min}$), it can be seen that

$$\begin{aligned} u_c &= K\left[e - f\left(u_c - u_{\max/\min}\right)\right] \\ &= (1 + Kf)^{-1} K\left(e + f u_{\max/\min}\right) \end{aligned}$$

Thus by choosing a constant f such that $|f| \gg 1$ and $|fK| \gg 1$,

$$\begin{aligned} u_c &\approx (fK)^{-1} K\left(e + f u_{\max/\min}\right) \\ &\approx u_{\max/\min} \end{aligned}$$

Therefore, during saturation, u_c is clamped at $u_{\max/\min}$ and wind-up is prevented, enabling the controller to come out of saturation as soon as e returns to normal levels.

This same arrangement ensures bumpless transfer in a multi-mode set-up. To show this, consider the set-up in Fig. 10b. At the time instant shown, k_1 is operating in closed loop while k_2 is operating in open loop. Thus

$$u_i = k_i[e - f_i(u_i - u)] = (1 + k_i f_i)^{-1} k_i (e + f_i u)$$

and

$$\hat{e}_i = k_i(e - f_i \hat{e}_i) - u = (1 + k_i f_i)^{-1}(k_i e - u)$$

If f_i values are chosen to be constant so that $|f_i| \gg 1$ and $|f_i k_i| \gg 1$, then $\hat{e}_i \approx 0$. This means that a bumpless transfer is possible as $u_i \approx u$. Once the switch is toggled, k_1 and k_2 exchange roles. Thus the same control scheme simultaneously achieves both bumpless transfer and anti-wind-up. In this design, a feedback gain f of 4.9 was used.

4.3.2 *Gain scheduling*

This plant could theoretically have been controlled via gain scheduling since the frequency responses are compatible for this purpose. A multi-mode scheme is, however, more general as there are situations where the system models are radically different (such as when the motor reverses) and a single compensator (such as a PI) cannot stabilize the plant over the entire loop by merely changing the gain. In addition, the multi-mode scheme allows for variable rate sampling at no extra cost and includes wind-up protection.

4.3.3 *RHP zeros*

In general, the closer the RHP zeros are to the imaginary axis, the more severe is their effect. In this application, the RHP zeros were far from the imaginary axes and as such do not pose a severe limitation to the design. Unfortunately, the locations of the RHP zeros depend on a variety of factors including the operating speed, length of pipes and fluid characteristics. As a result, their effect cannot be completely dismissed as there will be

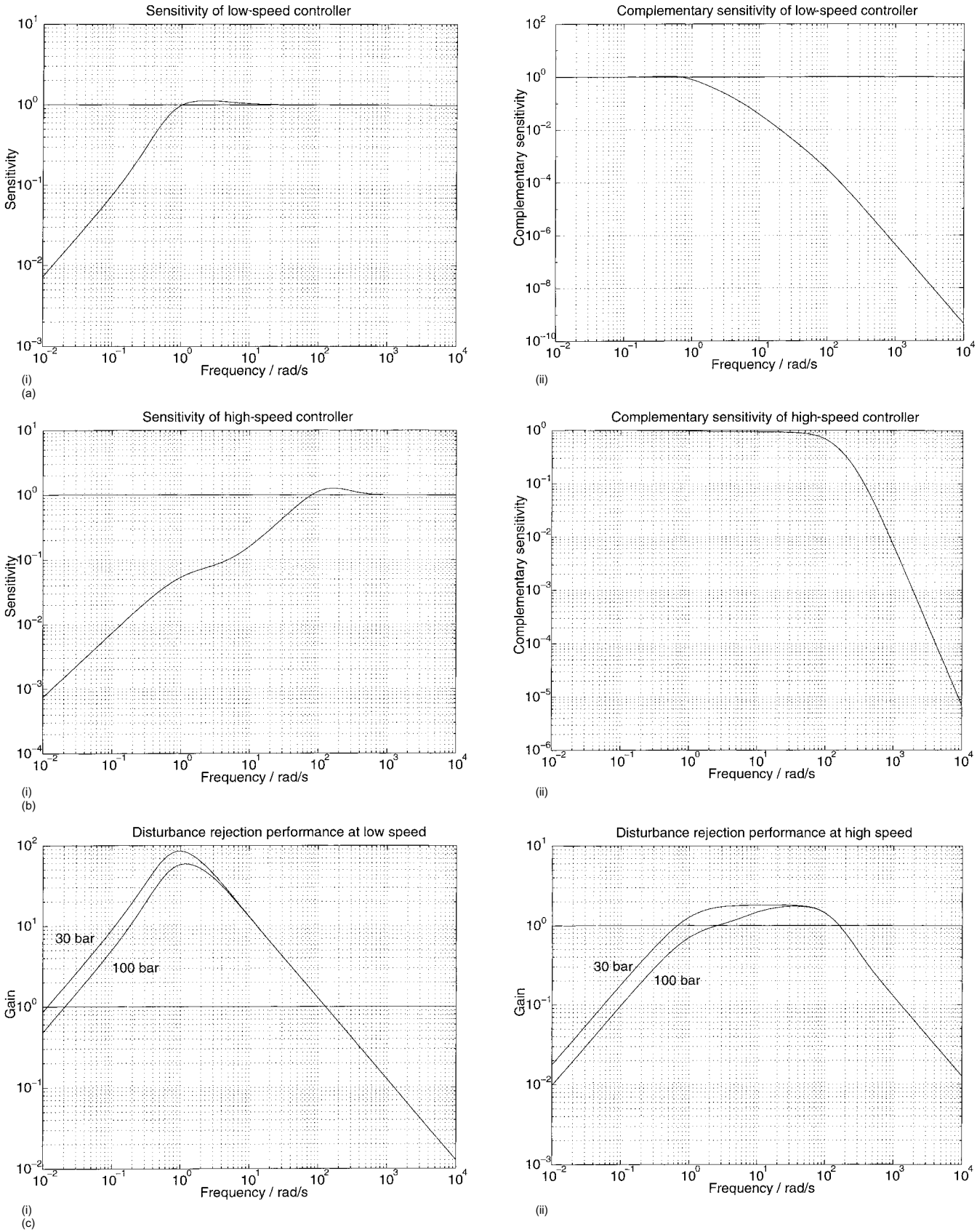

Fig. 9 (a)(i) Sensitivity of low-speed system; (ii) complementary sensitivity of low-speed system. (b)(i) Sensitivity of high-speed system; (ii) complementary sensitivity of high-speed system. (c)(i) Disturbance rejection performance at low speeds; (ii) disturbance rejection performance at high speeds

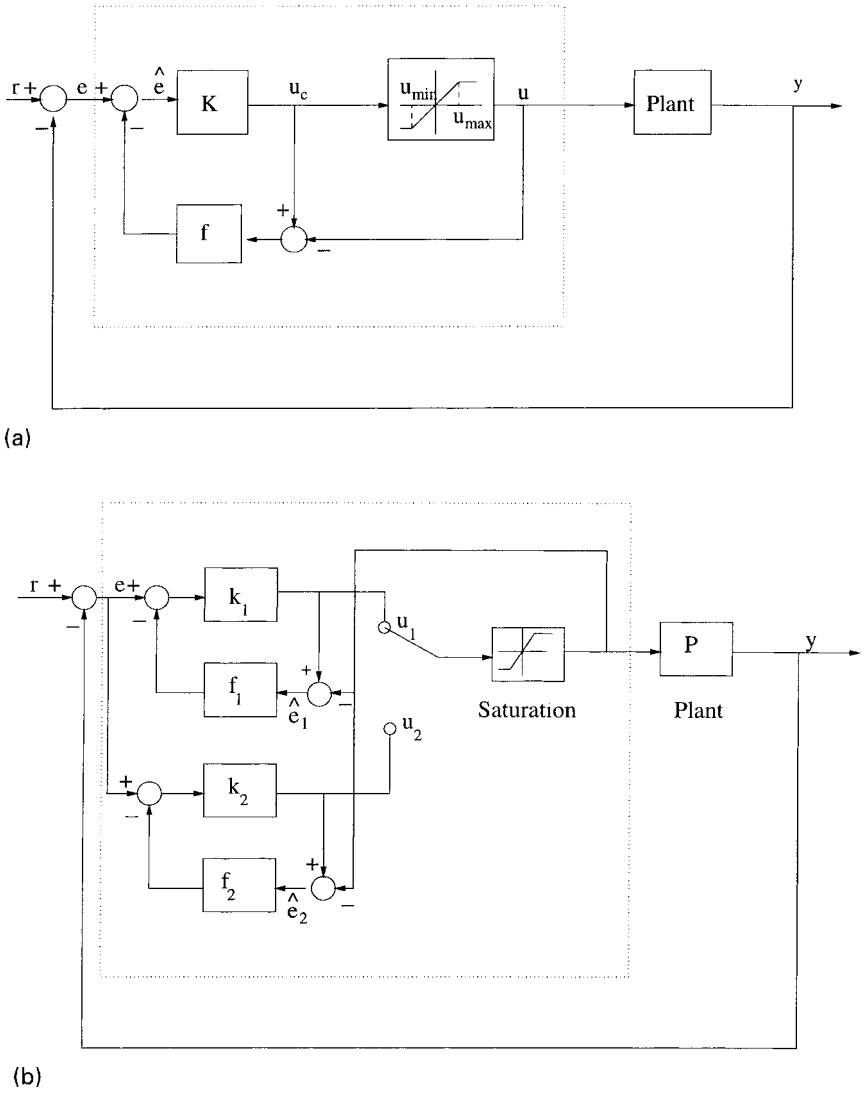

Fig. 10 (a) Anti-wind-up scheme to combat saturation problems. (b) Bumpless transfer scheme with anti-wind-up

circumstances where they could represent a limiting design constraint.

4.4 Comparison with a PID controller

Given that the pre-compensators used in the H_∞ design were simple PI compensators, and that significant model reduction was possible, there is the suspicion that adequate performance could have been achieved with PI controllers alone. We now compare the performance of equivalent PI compensators. The sensitivity as well as complementary sensitivity function for the PI approximate those of the loop shaping controller, leading to an identical nominal performance. Unfortunately, good nominal performance for a PI controller has no robust performance implications. This problem can be investigated using μ analyses.

4.4.1 The μ analyses of the closed-loop system

Comparing the performance of different controllers just by using their time responses can be highly limiting since exhaustive testing is required in order to quantify robust performance. However, the structured singular value μ provides a universal robust performance measure for closed-loop systems if the uncertainty structure is known. Here attempts are made to compare the relative performance of the H_∞ loop shape controller and a standard PID using μ analyses. Specific details on μ analyses can be found in reference [**12**].

The μ analyses for the loop-shaping controller are particularly conservative since the uncertainty structure used for testing does not encompass the full uncertainty admissible to the loop-shaping controller. Here, attempts will be made to approximate the parametric-type uncertainty in our system by an equivalent

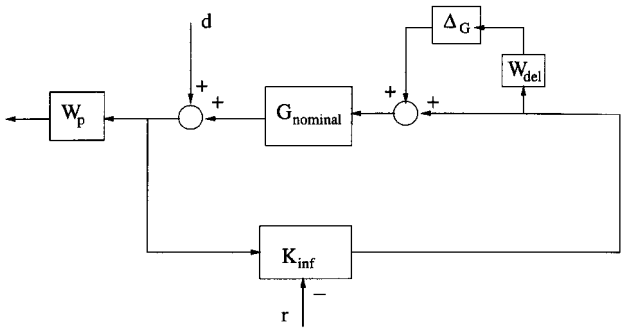

Fig. 11 Multiplicative uncertainty structure for μ analysis

multiplicative-type uncertainty and then to perform μ analyses on the perturbed system. The closed-loop interconnection structure in Fig. 11 is used. Looking at the family of plots in Fig. 2 we adopted for the high-speed controller a multiplicative uncertainty structure $W_{del} = 40(s + 100)/(s + 10\,000)$ which effectively admits a 40 per cent uncertainty at low frequencies up to about 50 rad/s and much higher at high frequencies. A performance weight of $W_p = 0.361\,64s + 17.094\,83/(s + 0.401\,88)$ is adopted and this ensures a disturbance rejection of 40 to 1 in the output channel at low frequencies, becoming less stringent at higher frequencies (above 10 rad/s).

The μ plot for these weights is shown in Fig. 12a for the loop-shaping and PI controllers. The loop-shaping controller outperforms the PI controller (lower value for μ) at all frequencies with the PI actually failing the test at about 0.7 rad/s. For the low-speed controller, $W_{del} = 20(s + 80)/(s + 8000)$ is selected and this represents an uncertainty of about 20 per cent at low frequencies, rising to over 100 per cent after 400 rad/s. The performance weight $W_p = (1.265\,6s + 0.416\,4)/(s + 0.075\,0)$ specifies a modest disturbance rejection of about 6 to 1 at low frequencies, and falling after 0.1 rad/s. The μ plot for these weights is shown in Fig. 12b for the loop-shaping and PI controllers. Here again, the loop-shaping controller outperforms the PI controller at all frequencies, with the PI controller failing hopelessly after 1 rad/s.

5 CONTROLLER TESTING

5.1 Discretization

Discretization is an important consideration in the loop-shaping controller. In this application, the Tustin method is used to discretize the controller. Of key importance is the selected discretization frequency. The recommended lower limit for the sampling frequency is generally of the order of ten times the process bandwidth and the upper limit (depending on the hardware) can be up to 50 times the bandwidth. For this process, the bandwith at low speeds falls to one-tenth of the bandwidth at high speeds. Thus, if the nominal frequency is used for sampling at either low or high speeds, operation at the other speed will be very different from the recommended sampling rate. Take for example the case where the system is sampled at the nominal rate for high speeds. Then at low speeds, the same rate will correspond to sampling at least 100 times the bandwidth. Theoretically, this problem can easily be seen from the solution of a discrete time system $\boldsymbol{y}(z) = \mathbf{C}[z\mathbf{I} - (\mathbf{I} + \mathbf{A}t_s)]^{-1}(t_s\mathbf{B}u(z) + z\boldsymbol{x}_0)$ which, for small sampling interval t_s, can lead to numerical problems as $\mathbf{I} + \mathbf{A}t_s$ is 'swamped' by $\mathbf{I}$ and dynamic information contained in $\mathbf{A}$ is lost. Due to the very large separation between the bandwidths, it might have been

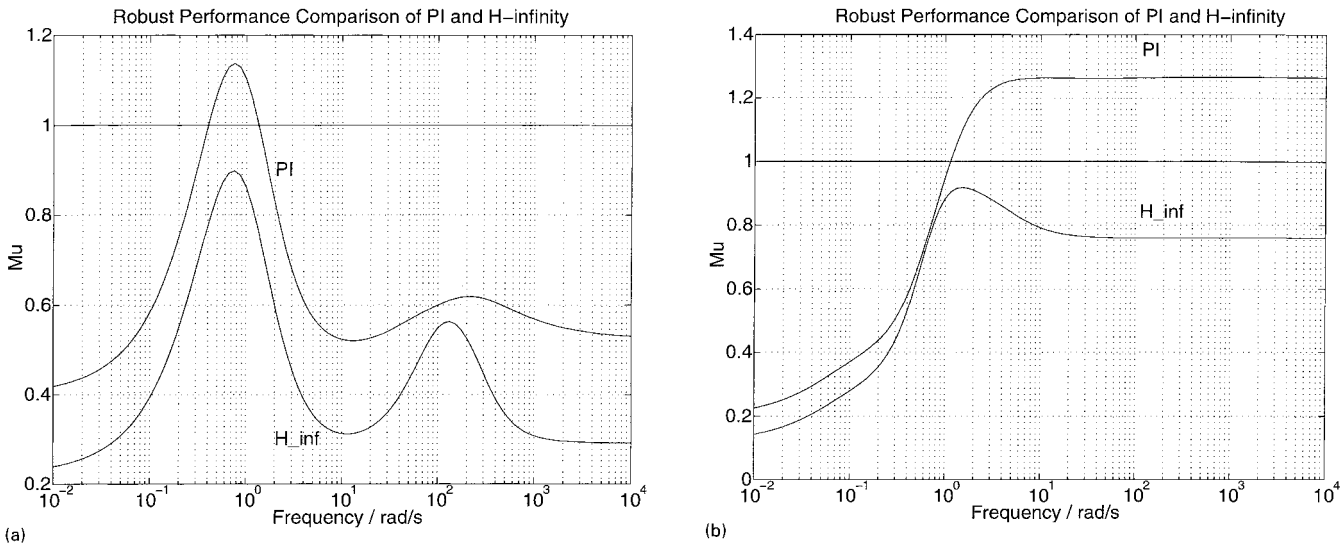

Fig. 12 μ plots for PI and loop-sharing controllers: (a) high speeds; (b) low speeds

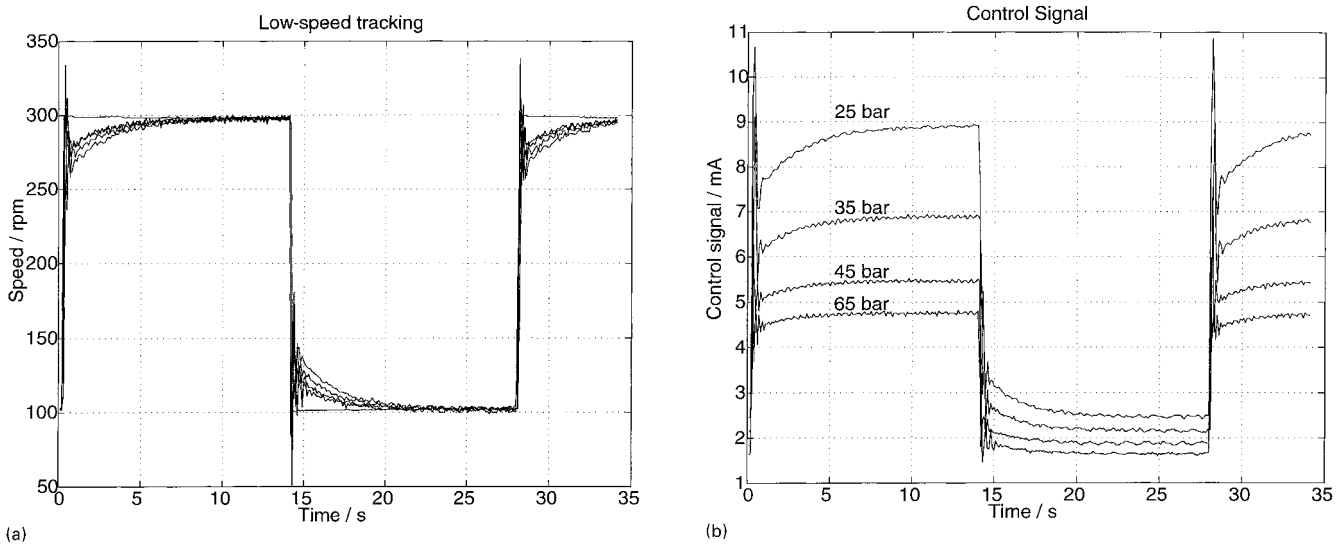

Fig. 13 (a) Set point tracking at low speeds. (b) Control signals for set point tracking at low speeds

difficult to select a compromise sampling rate without losing dynamic information but the proposed multi-mode scheme solves this problem rather naturally, with a dual sampling rate for the system. The high-speed process is sampled at 350 Hz and the low-speed process at 35 Hz. This is easily achieved in practice. In this case an internal counter was used to divide the sampling frequency by 10.

A decision also has to be made as to where the switching point of the controller lies since this will influence the stability and overall performance of the closed-loop system. Here the switching point is specified at 300 r/min with the motor maximum speed of about 2900 r/min. Thus the high-speed controller is active at all speeds above 300 r/min. The valve-rated current is 20 mA.

The controller was implemented in z transforms via a direct canonical realization of the transfer functions. The control program was written in C++ and implemented on a 133 MHz, 32 bit IBM personal computer with a DT21 input–output card. The high speed of the computer allowed the computational time of the algorithm to be taken as negligible.

5.2 Tracking tests

Figures 13 and 14 show the closed-loop response to set point changes for both low and high speeds respectively. The supply pressures for the low-speed case depicted in Fig. 13 were 25, 35, 45 and 65 bar. At very-low-speed set

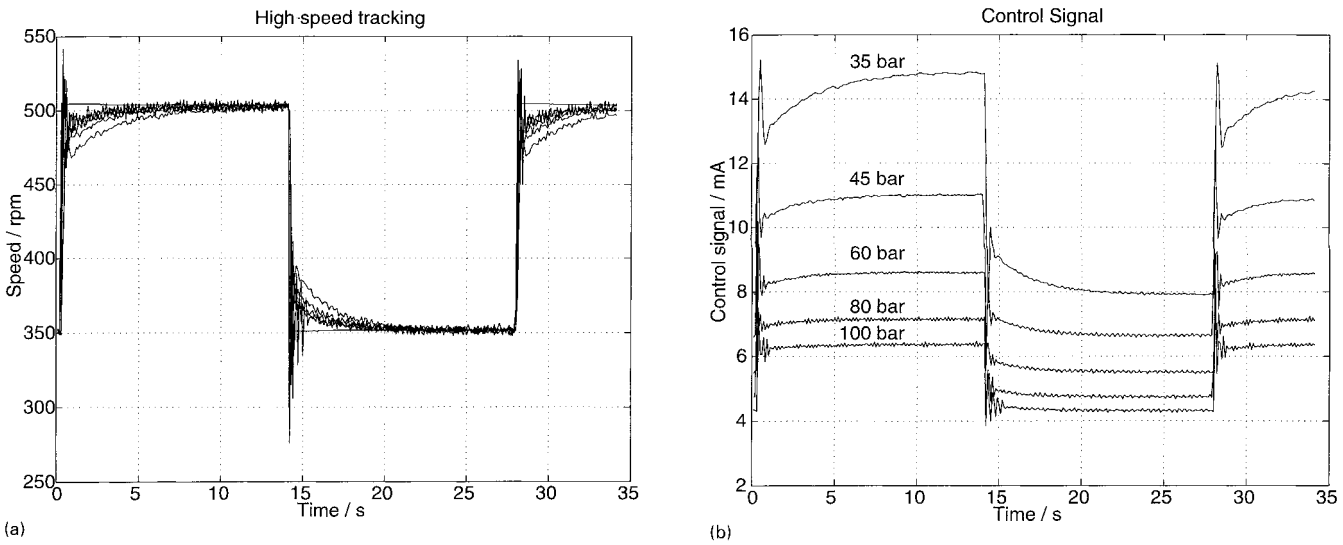

Fig. 14 (a) Set point tracking at high speeds. (b) Control signals for set point tracking at high speeds

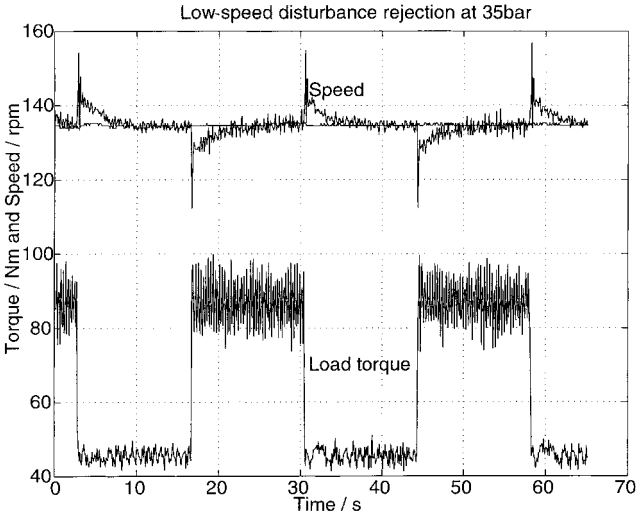

(i)
(a)

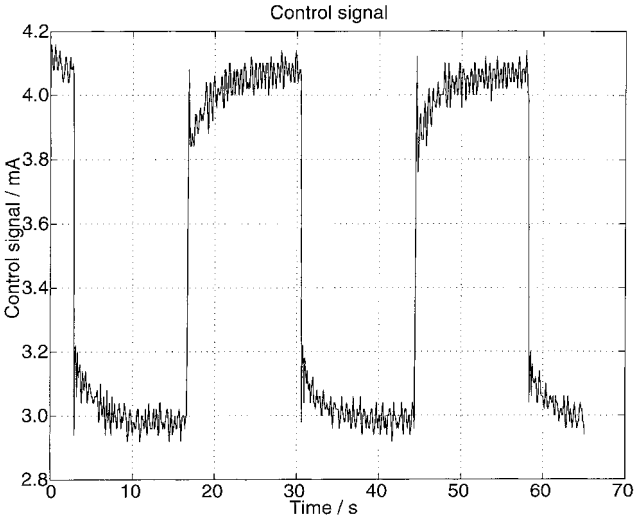

(ii)

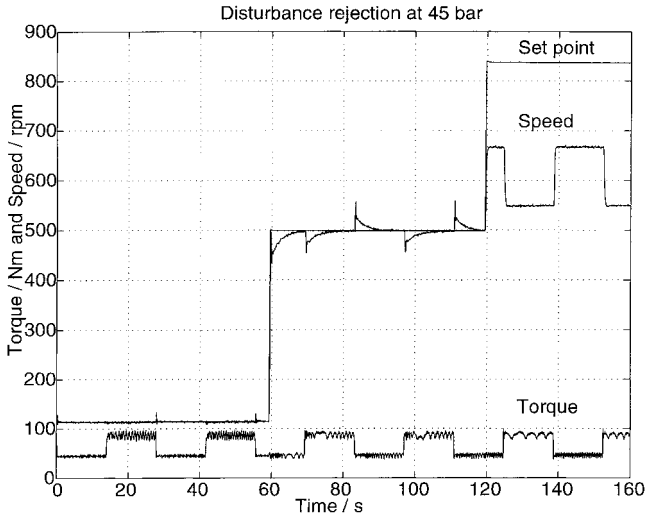

(i)
(b)

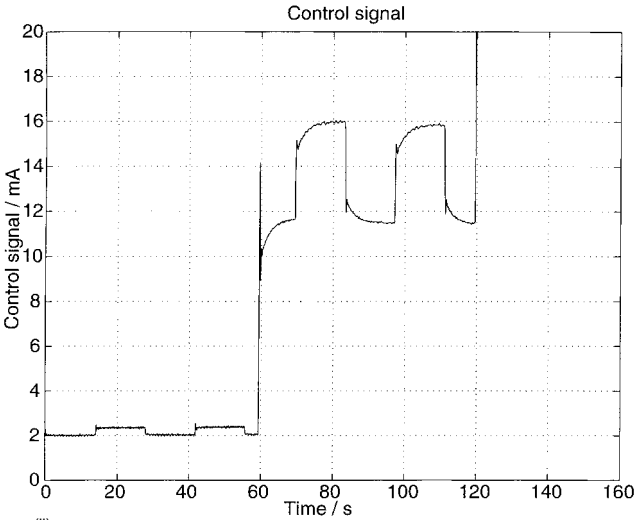

(ii)

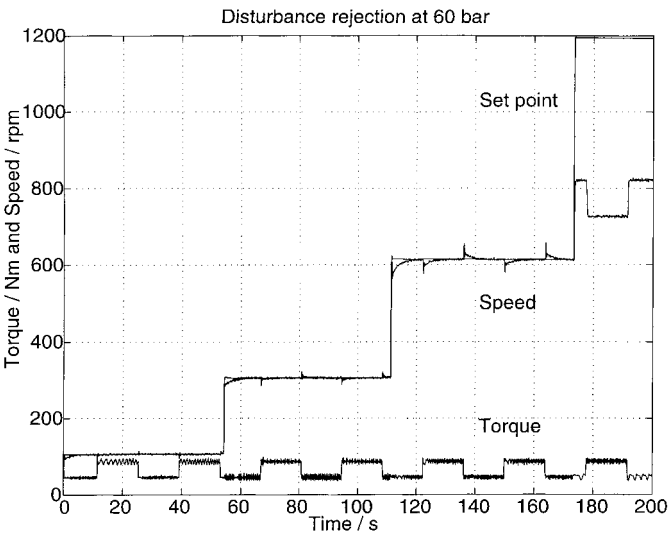

(i)
(c)

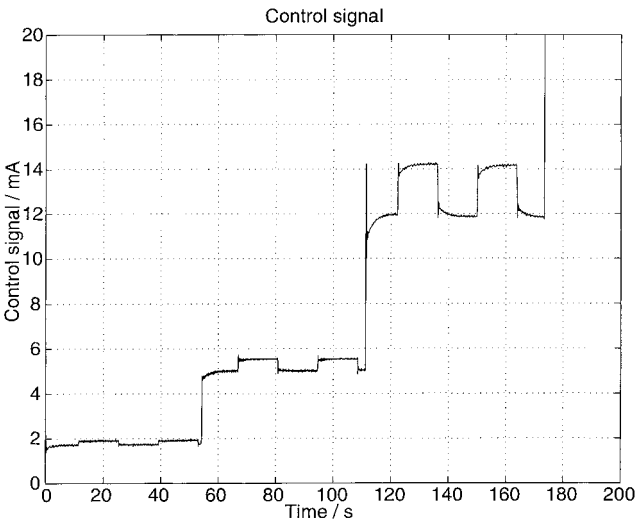

(ii)

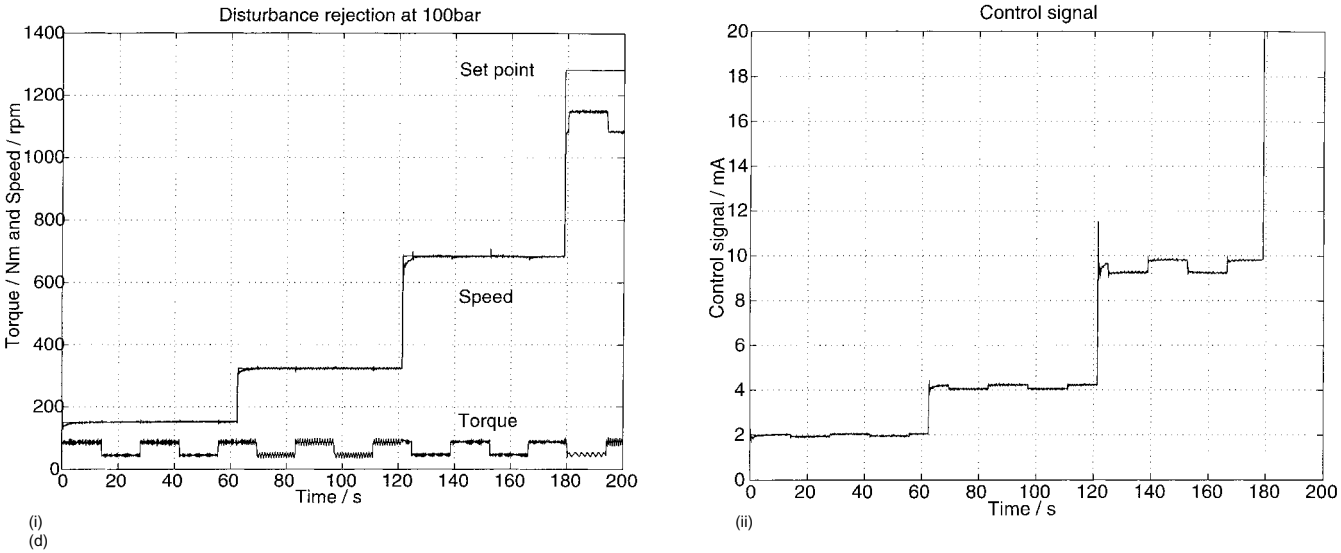

Fig. 15 (a)(i) Disturbance rejection at 35 bar; (ii) control signals for disturbance rejection at 35 bar. (b)(i) Disturbance rejection at 45 bar; (ii) control signals for disturbance rejection at 45 bar. (c)(i) Disturbance rejection at 60 bar; (ii) control signals for disturbance rejection at 60 bar. (d)(i) Disturbance rejection at 100 bar; (ii) control signals for disturbance rejection at 100 bar

points (under 60 r/min) the transient response (with the low-speed controller active) begins to deteriorate above 70 bar due to the high loop gain. The supply pressures for the high-speed case depicted in Fig. 14 were 35, 45, 60, 80 and 100 bar. The high-speed controller worked well up to a supply pressure of 120 bar. Judging from the control signals, the scheme is very effective as tracking is still maintained despite a doubling of loop gain over the operating conditions (Fig. 13b and 14b). The higher levels of control signal correspond to lower supply pressures since the corresponding lower loop gain demands a greater control signal and vice versa.

5.3 Disturbance rejection tests

Figure 15 shows for a range of pressures (35–100 bar) a collection of disturbance rejection tests at low, intermediate and high speeds, leading to saturation. Note the superb low-speed disturbance rejection (Fig. 15a), even at 35 bar. Note also how disturbance rejection improves with increasing supply pressure with the load hardly making any impression on the speed at 100 bar (Fig. 15d). It is possible to improve the disturbance rejection by reducing the sensitivity (e.g. by increasing the forward path gain).

Note that controller saturation leads to inability to reject disturbances (Figs 15c and d) when set point speeds are too high.

5.4 Bumpless transfer tests

With the switching point set at 300 r/min, the set point is moved so that alternate controllers are engaged. The supply pressures are 35, 45, 60, 80 and 100 bar. Figure 16 shows the responses of the system. A bumpless transition between the controllers can easily be observed. The corresponding control signals are shown in Fig. 16b.

5.5 Anti-wind-up test

Figure 17 shows the tracking response of the system. The set point is changed from 750 to 1290 r/min. At the operating pressure of 100 bar, a speed output of 1290 r/min is beyond the capability of the motor and leaves the controller saturated. The output can be seen to change immediately that the demand is reduced to 570 r/min as the controller comes out of saturation.

6 CONCLUSIONS

The feasibility of applying robust H_∞ control schemes to fluid power systems has been demonstrated on the speed control of a hydraulic motor. It has been shown that, despite the presence of significant feedback control problems, various control objectives can be achieved using a one-degree-of-freedom H_∞ controller. A multimode control scheme was proposed, which can be applied even where there is extreme model variation over the operating envelope, as a different controller is used at each operating region. In addition, performance can be optimized at each operating region and multirate sampling can be performed at little extra cost. This is important in digital implementation using z trans-

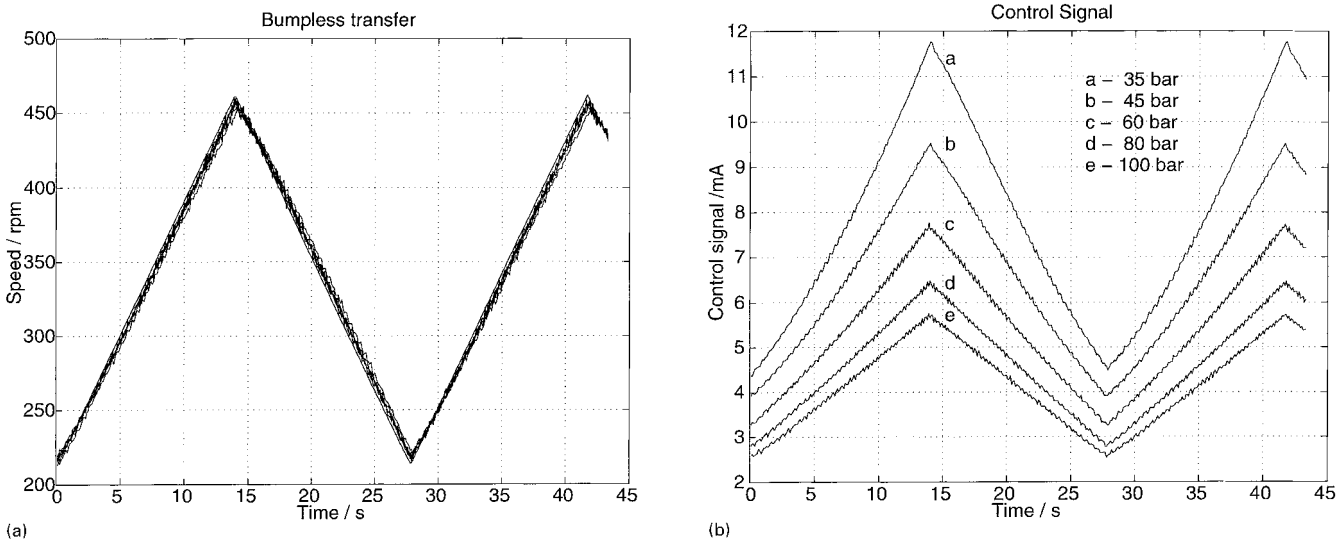

Fig. 16 Bumpless transfer tests: (a) set point tracking; (b) control signals

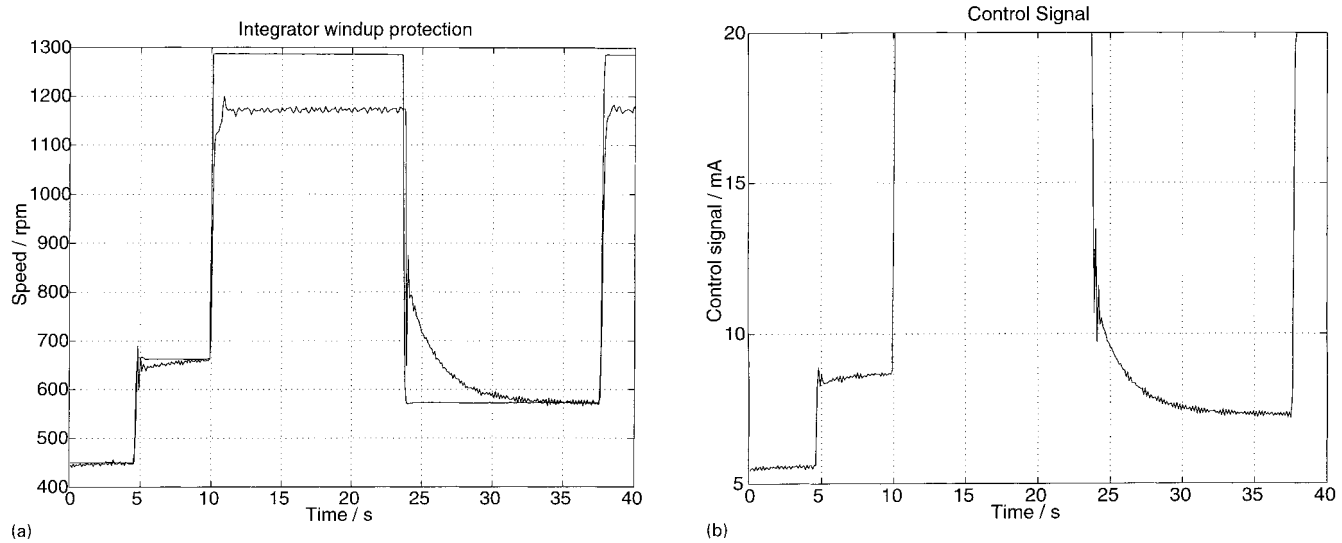

Fig. 17 Anti-wind-up performance of controller: (a) set point tracking; (b) control signal

forms, since the large bandwidth variation could lead to numerical problems.

Despite its rather modest order, the H_∞ loop-shaping controller was shown to offer superior performance to a PI controller with the same nominal performance. In addition to the assurance of robust stability, there is only a marginal increase in the design complexity of the H_∞ controller for multiple-input multiple-output systems as opposed to a PID controller. The apparent added complexity of this control system is outweighed by the added benefit of having the entire speed range available with robust performance. This, added to the low and ever-declining costs of electronic hardware, means that such controllers should in practice not be significantly more expensive than less sophisticated (PID) controllers.

Another important conclusion from this work is that it demonstrates the success that can be achieved when the benefits of advanced modelling packages are combined with those of modern robust control design tools in solving real problems in fluid power.

The work presented here provides a general approach to the design of fluid power systems which is capable of satisfying performance specifications in the presence of model uncertainty and system disturbances.

ACKNOWLEDGEMENTS

This work was supported by Engineering and Physical Sciences Research Council Grant GR/K38724. The authors are also grateful to Professor P. C. Young,

University of Lancaster, and H. El-Zobaidi, University of London, for useful discussions.

REFERENCES

1 **Backé, W.** The present and future of fluid power. *Proc. Instn Mech. Engrs, Part I, Journal of Systems and Control Engineering*, 1993, **207**(I4), 193–212.

2 **Isidori, A.** *Nonlinear Control Systems*, 2nd edition, 1989 (Springer-Verlag, Berlin).

3 **Vidyasagar, M.** *Nonlinear Systems Analyses*, 3rd edition, 1993 (Prentice-Hall, Englewood Cliffs, New Jersey).

4 **Burrows, C. R., Tomlinson, S. P.** and **Hogan, P. A.** Some modelling aspects of BATH*fp*. In *Fluid Power Systems Modelling and Control*, Proceedings of the Fourth Bath International Fluid Power Workshop (Eds C. R. Burrows and K. A. Edge), 1991, pp. 201–215.

5 **Vinnicombe, G.** Measuring robustness of feedback systems. PhD Dissertation, University of Cambridge, 1993.

6 **Zames, G.** Feedback and optimal sensitivity: model reference transformations, multiplicative seminorms and approximate inverses. *IEEE Trans. Automatic Control*, 1981, **AC-26**, 301–320.

7 **Itkis, U.** *Control Systems of Variable Structure*, 1976 (John Wiley, New York).

8 **Edge,K.A.** The control of fluid power systems—responding to the challenges. *Proc Instn Mech. Engrs, Part I, Journal of Systems and Control Engineering*, 1997, **211**(I2), 91–110.

9 **Piché, R., Pohjolainen, S.** and **Virvalo, T.** Design of robust two-degree-of-freedom controllers for position servos using *H*-infinity theory. *Proc. Instn Mech. Engrs, Part I, Journal of Systems and Control Engineering*, 1992, **206**(I2), 135–142.

10 **Hampson, S.** H_∞ control of a hydrostatic transmission. Report, University of Bath Fluid Power Centre, 1995.

11 **Piché, R., Pohjolainen, S.** and **Virvalo, T.** Design of robust controllers for position servos using *H*-infinity theory. *Proc. Instn Mech. Engrs, Part I, Journal of Systems and Control Engineering*, 1991, **205**(I4), 299–306.

12 **Skogestad, S.** and **Postlethwaite, I.** *Multivariable Feedback Control Analysis and Design*, 1995 (John Wiley, New York).

13 **Zhou, K., Doyle, J. C.** and **Glover, K.** *Robust and Optimal Control*, 1995 (Prentice-Hall, Englewood Cliffs, New Jersey).

14 **McFarlane, D.** and **Glover, K.** Robust controller design using normalised coprime factor plant descriptions. Lecture Notes in Control and Information Sciences, Vol. 138, 1990 (Springer-Verlag, Berlin).

15 **Green, M.** and **Limebeer, D. J. N.** *Linear Robust Control*, 1995 (Prentice-Hall, Englewood Cliffs, New Jersey).